Photocatalysis

Deutsche Ausgabe: DOI: 10.1002/ange.201508325
Internationale Ausgabe: DOI: 10.1002/anie.201508325

A Semi-Conductive Copper–Organic Framework with Two Types of Photocatalytic Activity

Zhi-Lei Wu[+], Chang-Hong Wang[+], Bin Zhao, Jie Dong, Feng Lu, Wei-Hua Wang, Wei-Chao Wang,* Guang-Jun Wu, Jian-Zhong Cui, and Peng Cheng*

Abstract: *Based on the newly designed ligand 4′-(3,5-dicarboxyphenyl)-4,2′:6′,4″-terpyridine (DCTP), a unique semi-conductive 3D framework $\{[Cu^{I}Cu^{II}_2(DCTP)_2]NO_3{\cdot}1.5\,DMF\}_n$ (**1**) with a narrow band gap of 2.1 eV, was obtained and structurally characterized. DFT calculations with van de Waals correction employed to explore the electronic structure of **1**, clearly revealed its semi-conductive behavior. Furthermore, we found that **1** exhibits a superior band alignment with water to produce hydrogen and degrade organic pollutants. Without adding any photosensitizers, **1** displays an efficiently photocatalytic hydrogen production in water based on the photo-generated electrons under UV/Vis light. **1** also exhibits excellent photo-degradation of methyl blue under visible-light owing to the strong oxidization of excited holes. It is the first example of MOFs with doubly photocatalytic activities related to photo-generated electrons and holes, respectively.*

With increasing concern about the problems of environmental pollution and energy, the photo-driven water splitting as a sustainable pathway for solar energy conversion, is receiving considerable attention, because photocatalytic hydrogen evolution, as a long-term alternative to replace fossil fuels, provides clear and high-performance energy sources.[1–3] In the past few years, various semiconductor materials were employed for photocatalytic hydrogen evolution. To be an ideal photoelectrode in the single-light-absorber setup, the semiconductor must satisfy several fundamental requirements, including suitable band alignment with water redox potentials, reasonable band gap (ca. 2.0 eV), long-term stability against the photo-corrosion in water.[4] In these studies, the metal–organic frameworks (MOFs) were first identified by Mori's group as a new class of materials for photocatalytic hydrogen production,[5] and recently the intense interests in this area have been focused on porous MOFs because of their large surface areas, small metal-oxide clusters, and the tunable band gaps.[6] To date, some hydrogen production photocatalysts based on MOFs have been explored, such as UiO-66, $[Ru_2(H_2TCPP)BF_4]$, $[Zn\{Pd(INA)_4\}]_n$, $[Zn_2(H_2O)_3\{PdCl_2(pydc)_2\}]_n$, Pt/MIL-101.[7] The UiO-66 was tested as a good photocatalyst for hydrogen evolution in a methanol/water mix solution, and enhanced activity was observed when Pt nanoparticles were introduced as co-catalysts into the framework. Most of the photocatalytic water splitting into hydrogen based on MOFs materials was realized by employing an additional photosensitizer, such as $[Ru(bpy)_3]^{2+}$, methyl viologen, or RhB, and simultaneously, the metal ions in constructing the MOFs mentioned above are almost focused on expensive metals Ru, Pd, Ti, and Zr. Therefore, to avoid using additional photosensitizers and expensive metals, it is crucial and necessary to seek new MOF photocatalysts constructed from cheap metal ions, such as Cu, Zn, and organic ligands with large electron delocalization systems as effective photosensitizers. Importantly, to our knowledge, MOF materials with doubly photocatalytic activities in splitting water into hydrogen by using photo-generated electrons and degrading organic pollutant based on holes, have not been reported so far.

Herein, based on a newly designed ligand 4′-(3,5-dicarboxyphenyl)-4,2′:6′,4″-terpyridine (DCTP, synthesis was given in Supporting Information, the structure is shown in Figure S1), a novel semi-conductive copper–organic framework $\{[Cu^{I}Cu^{II}_2(DCTP)_2]NO_3{\cdot}1.5\,DMF\}_n$ (**1**) was synthesized and structurally characterized. Theoretical calculations of the electronic structure and work function display that this specific compound shows a semiconducting behavior ($E_g =$ 2.1 eV) with a superior band alignment with water redox potentials to produce hydrogen and degrade organic pollutants. Experimentally, this compound is shown to exhibits efficient photocatalytic hydrogen evolution and degradation of organic dyes.

Single-crystal X-ray diffraction analyses revealed that compound **1** is a 3D twofold interpenetrated framework with mixed-valence dinuclear Cu subunits, crystallizing in monoclinic space group *C*2/*c*. The asymmetric unit consists of one Cu^{II} ion, half of one Cu^{I} ion, and one DCTP anion. The two crystallographically independent Cu^{I} and Cu^{II} ions form a "paddle-wheel"-type motif with only two carboxyl bridges (Figure 1 a), rather than the standard "paddle-wheel" arrangement bridged by four carboxyl groups. In the dinuclear Cu subunits, the Cu^{I} is two-coordinated by two oxygen

[*] Z.-L. Wu,[+] Prof. Dr. B. Zhao, J. Dong, Dr. G.-J. Wu, Prof. Dr. P. Cheng
Department of Chemistry, Key Laboratory of Advanced Energy Material Chemistry, Nankai University and Collaborative Innovation Center of Chemical Science and Engineering (Tianjin)
Tianjin 300071 (China)
E-mail: zhaobin@nankai.edu.cn
C.-H. Wang,[+] Dr. F. Lu, Dr. W.-H. Wang, Prof. Dr. W.-C. Wang
College of Electronic Information and Optical Engineering
Nankai University
Tianjin 300071 (China)
E-mail: weichaowang@nankai.edu.cn
Z.-L. Wu,[+] Prof. Dr. J.-Z. Cui
Department of Chemistry, Tianjin University
Tianjin 300072 (China)
[+] These authors contributed equally to this work.

Supporting information for this article is available on the WWW under http://dx.doi.org/10.1002/anie.201508325.

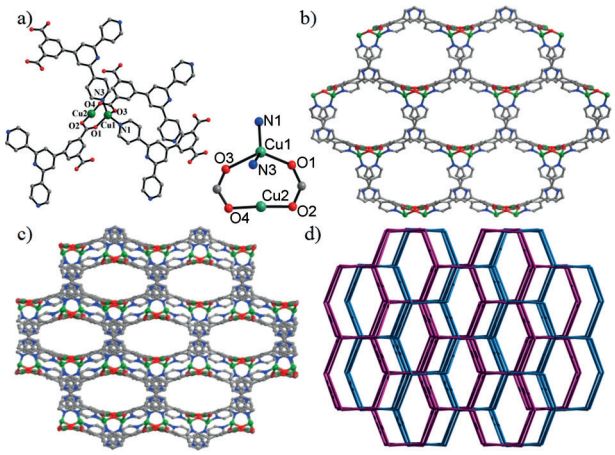

Figure 1. a) The coordination environments of the copper atoms in compound **1**. b) One net of the 3D framework and c) twofold interpenetrating 3D framework in **1** viewed along the *c* axis (C gray; N blue; O red; H atoms and free DMF molecules are omitted for clarity). d) The simplified topological structure, colors indicate the two nets.

atoms (O2 and O4) from different carboxyl groups of the $DCTP^{2-}$ anions. The four-coordinated Cu^{II} center displays a tetrahedral coordination environment, which is formed by two carboxylic oxygen atoms (O1 and O3) and two nitrogen atoms (N1 and N3) from four $DCTP^{2-}$ anions. The two-coordinate Cu(I) center has never been reported in similar mixed-valence dinuclear copper compounds,[8] and provides a potential catalytic platform. The Cu–Cu distance is 3.014 Å. All the dinuclear subunits are linked by $DCTP^{2-}$ anions to form a 3D framework (Figure 1b), then two nets of the independent 3D frameworks interpenetrate each other, exhibiting a one-dimensional channel along the *c* axis (Figure 1c). The regular window of the channel is 13.96×6.95 Å^2. Upon solvent removal, the total solvent-accessible volume is approximately 23.2%, calculated with PLATON software.[9] However, owing to the low N_2 absorption capacity at 77 K, the surface area of **1** was not experimentally determined (Figure S2). The network topology of **1** is also investigated by the computer program TOPOS.[10] The dinuclear Cu subunit is considered as a four-connected node which is linked by four $DCTP^{2-}$ anions, and the whole structure can be simplified as a 4-connected **neb** topology, with the Schläfli symbol of 6^6 and the vertex symbol of $(6{\cdot}6{\cdot}6{\cdot}6_2{\cdot}6_2{\cdot}6_2)$ and $(6{\cdot}6{\cdot}6{\cdot}6_2{\cdot}6_2{\cdot}6_2)$ (Figure 1d).

The oxidation states of Cu ions are further confirmed by X-ray photoelectron spectroscopy (XPS). The XPS spectra of **1** show the characteristic peaks of $2p_{3/2}$ and $2p_{1/2}$ at 932.4 and 952.3 eV, respectively, indicating the presence of Cu^{I} in **1**, and the remaining peaks at 939.4 and 960.4 eV correspond to the Cu^{II} ions in compound **1** (Figure S3).[11]

To explore the solvent stability of **1**, the powder X-ray diffraction (PXRD) pattern of **1** dispersed in various solvents for 12 h, including acetone, methanol, ethanol, CH_3CN, DMF, DMA, CH_2Cl_2, and DMSO, was performed at room temperature (Figure S4). The simulated PXRD of **1** coincided with the corresponding experimental ones, indicating that **1** has excellent solvent stability. Additionally, thermogravimetric analysis (TGA) was carried out in the temperature range of 30–800 °C (Figure S5). It displays a weight loss of 10.3% from room temperature to 245 °C, corresponding to the release of guest DMF molecules. The framework is stable up to about 300 °C, indicative of good thermal stability of compound **1**.

The investigation on UV/Vis spectra of ligand DCTP and **1** revealed that the adsorption band of DCTP in **1** appears red-shift, maybe caused by the effect of coordinated Cu ions on the excited state of the ligand. The weak band between 600 and 800 nm arises from the d–d transitions of the Cu^{2+} in **1** (Figure S6). The diffuse reflectance spectra of **1** was also studied (Figure S7), and the band-gap energy (E_g) of **1** determined from Tauc plot is 2.1 eV, which is more smaller than TiO_2 (3.2 eV for anatase and 3.0 eV for rutile) and some other reported MOFs, such as MIL-125-NH_2 (2.6 eV), UiO-66 (3.05 eV), and MIL-125 (3.6 eV), but slightly larger than MOF NTU-9 (1.72 eV) and MIL-88A (2.05 eV).[7a,12] The result revealed that **1** can be considered as an ideal semiconductive MOFs material and that such a low E_g value is rare for a MOF.

To understand the fundamental electronic structures of **1**, first-principles calculations were performed by density-functional theory (DFT), as implemented in plane-wave basis code Vienna ab initio Simulation Package (VASP). The generalized gradient approximation (GGA) in the Perdew–Burke–Ernzerhof (PBE) forms was employed. It is well known that DFT underestimates the band gap of semiconductor materials, a screened-exchange hybrid functional Heyd–Scuseria–Ernzerhof (HSE) was thus used to resolve this issue. Additionally, the standard GGA-type density functions are unable to describe the weak long distance interactions, and an empirical dispersion-corrected density functional theory (DFT-D2) method proposed by Grimme was thus adopted in our calculations. The model of **1** was constructed based on the single-crystal X-ray diffraction analyses (Figure S8). As the directivity of solvent in the channel of **1** is uncertain, solvent is not included in our model.

As illustrated in Figure 2, compound **1** indicates an insulating behavior with a band gap of 2.04 eV, which is consistent with UV/Vis results. Local density of states (LDOS) and partial density of sates (PDOS; Figure S9) analysis display that the valance-band maximum (VBM) is mainly composed of Cu 3d orbitals. The conduction-band minimum (CBM) is dominated by 2p orbitals of C and N.

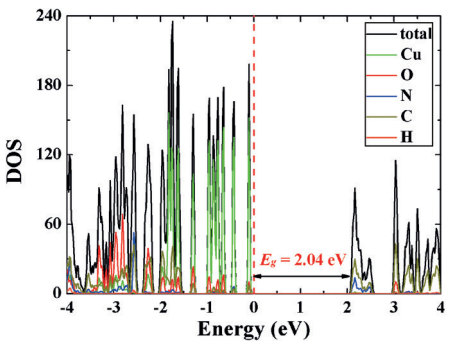

Figure 2. Normalized total and partial DOS of compound **1**. The Fermi level is at 0 eV.

When compound **1** is solar irradiated, the carriers are excited. Consequently, electrons jump into conduction band (CB) and holes are generated in valence band (VB). Intuitively, the excited electrons produced by Cu transfer to its neighboring C and N atoms, leaving Cu as the active site to provide holes. To predict the photocatalytic activity, band alignment with the water redox potentials is required. Herein, we set the vacuum level as the reference, and the work function of **1** needs to be precisely determined to essentially attain the energy-level alignments between compound **1** and water.

Theoretically, it is a long-term challenge to obtain the work function of MOF materials. Thanks to recent contribution from Butler, et al.,[13] it is now feasible to calculate the work function of MOF structures with a large porous diameter. In their work, the vacuum potential reaches a constant with an error range of 0.1 eV (0.01 eV) when the pore radii is as large as 5 Å (8 Å). In our work, we adopt this method to explore the structure of **1**. The spherical average of the electrostatic potential was calculated [Eq. (1)]:

$$\Phi_{av}(r) = \frac{1}{V}\int_V \Phi(r')d^3r' \quad (1)$$

where V and r are the volume and radius of the sphere, respectively.

With the distribution of electrostatic potentials, work function of **1** could be determined from the valence-band edge. Noted that this method would be valid for materials with a porous diameter larger than 1 nm. Nevertheless, the pores in **1** displays an ellipse shape with a shortest diameter of 0.7 nm, which definitely decreases the work function. To suppress this issue, we randomly scanned over 50 different electrostatic potentials (left panel in Figure 3) within the pore to obtain a highest work function which is ultimately close to the real value. From Figure 3, the work function of 5.3 eV was derived, and this value is in principle smaller than real one. In any case, we adopted this value for further analysis of photocatalytic origin. We aligned the water redox potentials with the band structures of **1**. Interestingly, we found that the conduction-band minimum of **1** is higher than H^+/H_2 level and Cu^I valance-band maximum is lower than O_2/H_2O energy level.[14] As a result, when this material is exposed to solar radiation, the photo-generated electrons transfer into H^+/H_2 to reduce H^+ into H_2, and OH^- is oxidized into O_2 with the help of excited holes. From the photocatalytic point of view, Cu^I serves as the active point to provide holes and its neighboring C and N atoms are the sites to accept electrons. One point that caught our attention is that we underestimated the work function based on current calculation methods. In practice, the Cu^I VBM should be even lower than the OH^- oxidation level, and in other words, the photocatalytic performance should be even better and the photocatalytic mechanism we proposed should not change even if the work function is underestimated here. These results imply that **1** can be expected to have bifunctional photocatalytic activity in water splitting and photo-degradation of organic pollutants.

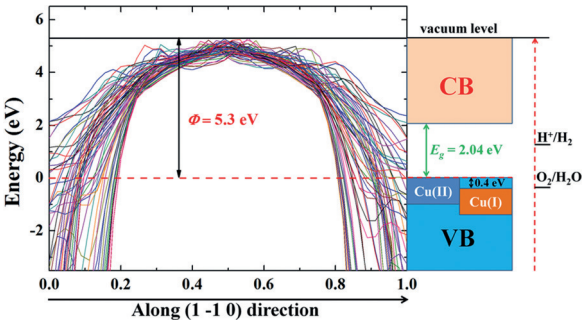

Figure 3. Linear scan of the spherical average electrostatic potential across the pore of compound **1**. Fermi level locates at 0 eV.

Based on the above theoretical investigations, the photocatalytic hydrogen evolution reactions were performed over **1** under UV-visible-light irradiation with methanol as a sacrificial agent and H_2PtCl_6 (1 mL, 0.1 wt %) as a co-catalyst. The amount of H_2 generated from the system increases with time (Figure S10), and reaches about 160 μmol g^{-1} with 5 h irradiation. In contrast, no detectable hydrogen was observed under only addition of H_2PtCl_6 and without **1** (Figure 4),

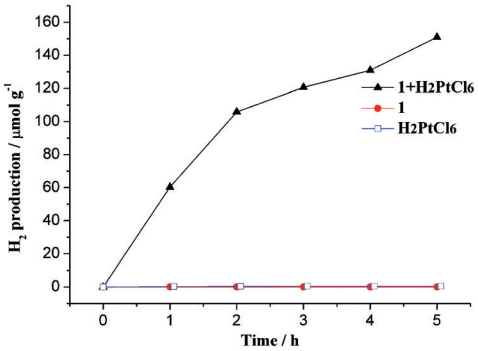

Figure 4. Photocatalytic H_2 production over **1** + H_2PtCl_6, **1**, and H_2PtCl_6.

indicating that compound **1** plays a crucial role in the photocatalytic reaction. After completing the photocatalytic hydrogen evaluation, the powder **1′** was characterized by X-ray photoelectron spectroscopy (XPS) and PXRD. In the XPS spectra of **1′**, the peaks at 71.1 and 74.8 eV can be clearly observed (Figure S11), corresponding to Pt $4f_{7/2}$ and Pt $4f_{5/2}$,[15] which indicates that Pt has been embedded onto frameworks of **1**. By comparison, the oxidation states of Cu ions do not change (Figure S3). The PXRD patterns of **1′** are consistent with the experimental and simulated ones of **1** (Figure S12), suggesting the introduction of Pt onto framework have no significant influence on the crystallinity and 3D frameworks of **1**. The absence of the characteristic Pt peak in the PXRD pattern was due to the low Pt loadings. Moreover, the morphology of the Pt in **1′** was further characterized by scanning electron microscope (SEM) and energy dispersive spectroscopy (EDS). As shown in Supporting Information Figures S13 and S14, the results indicate that the Pt was dispersed onto the framework of compound **1** as nanoparticles (NPs). Furthermore, when the reaction was performed for 7 h, the framework of **1** is still stable, confirmed by

the results of PXRD (Figure S15). However, the evolution rate slightly decreased (Figure S16), mainly due to the decrease in the concentration of sacrificial electron donor. The apparent quantum efficiency of **1** was calculated to be 2.3% at 420 nm, which is higher than the material GC40 (QE = 0.6%),[16] but lower than that of [2Fe2S]-based catalysts (QE = 18–28%).[17]

The possible mechanism for H_2 production of this system is illustrated in Supporting Information Scheme S1. When the UV/Vis light is absorbed by the organic linker of **1**, the excited photoelectron is formed and transfer to the Pt centers as a result of the lower Fermi level locations of Pt. Subsequently, the protons which gather on the surface of MOF by hydrogen bonding are transferred to the Pt centers or unsaturated Cu^I by water, and react with the photoelectrons to produce H_2. In this system, the compound **1** serves as a photo-electron generator to enhance the activity of H_2 production, and the Pt centers are good electron traps and can inhibit the recombination of photogenerated electrons and holes, providing redox reaction sites for hydrogen evolution and lower the over potential.

To date, various MOFs-based photocatalysts were used in photocatalytic hydrogen generation, [2c,7,18] extending the applications of MOFs into the photocatalysis field (Table S2). Mori and co-workers detect the photochemical reduction of water into hydrogen in a multicomponent system consisting of MOFs, $[Ru(bpy)_3]^{2+}$ as a photosensitizer, methyl viologen, and EDTA-2Na.[5] Li et al. incorporate Pt NPs and Au NPs into NH_2-MIL-125(Ti) to inhibit the recombination of photogenerated electrons and holes in MOFs, promoting the photocatalytic hydrogen evolution to different degrees.[18a] Moreover, He and co-workers embedded Pt NPs into the cavities of Zr-based MOFs for hydrogen evolution with RhB as photosensitizers.[7a] Below, we demonstrate that compound **1** based on comparatively cheap copper metal exhibits an efficient photocatalytic behavior without any photosensitizers.

According to the calculation results, **1** may serve as a catalyst to degrade organic dyes. Thus the catalytic degradation of methylene blue (MB) in aqueous solution (10 mg L^{-1}) in the presence of visible light was carried out. The photocatalytic activity of compound **1** was monitored by measuring maximum absorbance of MB at 590 nm (Figure S17). The concentration of MB is nearly unchanged in the absence of visible light and compound **1**, and only slight MB degradation was observed under light irradiation. In contrast, 70% of the MB can be decomposed under the introduction of **1** without visible light. Interestingly, up to 80% MB is decomposed under the presence of both **1** and visible light (Figures S18 and S19a). After repeating the photocatalytic degradation of MB three times, the solid residues in the reaction still displayed a similar photocatalytic efficiency as that of **1** (Figures S19b and S20–S22). Furthermore, the kinetics for MB degradation were also investigated. To our knowledge, not much effort has been devoted to kinetic studies for this system.[19] The data for MB degradation was fitted with first- and second-order reaction rate equations. The plots of $-\ln([A_t]/[A_0])$ and $1/[A_t]-1/[A_0]$ versus time are shown in the Supporting Information Figure S23, and the relationship of $1/[A_t]-1/[A_0]$ versus time displays a straight line, suggesting the MB degradation obeys a second-order process. Owing to the large size of the dye molecule, it is very difficult for MB to completely enter into the pore of **1** (Figure S24). The degradation mechanism for MB could be explained based on the semiconductor theory, which has been confirmed by the theoretical calculation above. The excited photo-electron moves from the VB to the CB when **1** is under illumination, meanwhile, the excited holes in the VB at the Cu^I sites help produce hydroxyl radicals (·OH) along with other oxidants, such as O_2^-, H_2O_2, to decompose the organic pollutants.

In summary, a novel $Cu^{I/II}$-based two-fold interpenetrated MOF was synthesized and structurally characterized. Compound **1** displays strong absorption in the visible light region with a narrow band gap of 2.1 eV, making it a potential semiconductive MOF material. Theoretical studies, based on the calculations of the work function of MOFs, exhibited a good band alignment with the water redox energy levels. The results revealed that **1** is an efficient catalyst in the photocatalytic hydrogen evolution reaction without adding photosensitizers. MOF **1** has also been demonstrated to display promising visible-light-driven catalytic activity in degrading MB. To our knowledge, it is the first report that MOF materials display two photocatalytic activities through employing photo-generated electrons and holes.

Experimental Section

1: A mixture of DCTP (0.0397 g, 0.1 mmol), $Cu(NO_3)_2{\cdot}6H_2O$ (0.0483 g, 0.2 mmol), DMF (5 mL), and 65% HNO_3 (200 μL) was sealed in a Teflon-lined stainless vessel (25 mL) and heated at 160 °C for 48 h, and then the vessel was cooled slowly to room temperature at 5 °C h^{-1}, affording as red needle like crystals. The yield was 76% based on the ligand DCTP. Elemental analysis (%) calcd for $C_{50.5}H_{36.5}Cu_3N_{8.5}O_{12.5}$: C 52.62, H 3.16, N 10.33; found: C 52.49, H 2.97, N 10.43. Crystal data from single-crystal diffraction studies for DCTP and **1** are given in Supporting Information.

Acknowledgements

This work was supported by 973 Program (2012CB821702), NSFC (21571107, 21421001, 11304161), SFC of Tianjin (15JCZDJC37700 and 13JCYBJC41100), and the China and the Fundamental Research Funds for the Central Universities 111 project (B12015), MOE Innovation Team (IRT13022 and IRT-13R30).

Keywords: DFT calculations · hydrogen generation · photocatalysis · photo-generated electrons and holes · semi-conductive MOFs

How to cite: *Angew. Chem. Int. Ed.* **2016**, *55*, 4938–4942
Angew. Chem. **2016**, *128*, 5022–5026

[1] a) Z. Zou, J. Ye, K. Sayama, H. Arakawa, *Nature* **2001**, *414*, 625–627; b) T. Zhang, W. B. Lin, *Chem. Soc. Rev.* **2014**, *43*, 5982–5993; c) Q. J. Xiang, J. G. Yu, M. Jaroniec, *J. Am. Chem. Soc.* **2012**, *134*, 6575–6578.

[2] a) J. Sato, N. Saito, Y. Yamada, K. Maeda, T. Takata, J. N. Kondo, M. Hara, H. Kobayashi, K. Domen, Y. Inoue, *J. Am. Chem. Soc.* **2005**, *127*, 4150 – 4151; b) X. Wang, K. Maeda, A. Thomas, K. Takanabe, G. Xin, J. M. Carlsson, K. Domen, M. Antonietti, *Nat. Mater.* **2009**, *8*, 76 – 80; c) S. L. Li, Q. Xu, *Energy Environ. Sci.* **2013**, *6*, 1656 – 1683.
[3] a) S. Min, G. Lu, *J. Phys. Chem. C* **2011**, *115*, 13938 – 13945; b) K. Sayama, K. Mukasa, R. Abe, Y. Abe, H. Arakawa, *Chem. Commun.* **2001**, 2416 – 2417.
[4] K. Maeda, K. Domen, *J. Phys. Chem. Lett.* **2010**, *1*, 2655 – 2661.
[5] Y. Kataoka, K. Sato, Y. Miyazaki, K. Masuda, H. Tanaka, S. Naito, W. Mori, *Energy Environ. Sci.* **2009**, *2*, 397 – 400.
[6] a) H. Q. Pham, T. Mai, N. N. Pham-Tran, Y. Kawazoe, H. Mizuseki, D. Nguyen-Manh, *J. Phys. Chem. C* **2014**, *118*, 4567 – 4577; b) M. D. Allendorf, A. Schwartzberg, V. Stavila, A. A. Talin, *Chem. Eur. J.* **2011**, *17*, 11372 – 11388; c) R. Lin, L. J. Shen, Z. Y. Ren, W. M. Wu, Y. X. Tan, H. R. Fu, J. Zhang, L. Wu, *Chem. Commun.* **2014**, *50*, 8533 – 8535.
[7] a) J. He, J. Q. Wang, Y. J. Chen, J. P. Zhang, D. L. Duan, Y. Wang, Z. Y. Yan, *Chem. Commun.* **2014**, *50*, 7063 – 7066; b) K. Sato, Y. Kataoka, W. Mori, *J. Nanosci. Nanotechnol.* **2012**, *12*, 585 – 590; c) Y. Miyazaki, Y. Kataoka, Y. Kitagawa, M. Okumura, W. Mori, *Chem. Lett.* **2010**, *39*, 878 – 880; d) Y. Miyazaki, Y. Kataoka, W. Mori, *J. Nanosci. Nanotechnol.* **2012**, *12*, 439 – 445; e) M. C. Wen, K. Mori, T. Kamegawa, H. Yamashita, *Chem. Commun.* **2014**, *50*, 11645 – 11648.
[8] a) M. L. Tong, L. J. Li, K. Mochizuki, H. C. Chang, X. M. Chen, Y. Li, S. Kitagawa, *Chem. Commun.* **2003**, 428 – 429; b) S. M. F. Lo, S. S. Y. Chui, L. Y. Shek, Z. Y. Lin, X. X. Zhang, G. H. Wen, I. D. Williams, *J. Am. Chem. Soc.* **2000**, *122*, 6293 – 6294.
[9] A. L. Spek, *J. Appl. Crystallogr.* **2003**, *36*, 7 – 13.
[10] a) V. A. Blatov, *IUCr Comp. Commun. Newslett.* **2006**, *7*, 4; b) V. A. Blatov, http://topospro.com/; c) M. O'Keeffe, Reticular Chemistry Structure Resource. http://rcsr.anu.edu.au/.
[11] Y. Zhu, W. Y. Wang, M. W. Guo, G. Li, H. J. Lu, *Inorg. Chem. Commun.* **2011**, *14*, 1432 – 1435.
[12] a) C. H. Hendon, D. Tiana, M. Fontecave, C. Sanchez, L. D'arras, C. Sassoye, L. Rozes, C. Mellot-Draznieks, A. Walsh, *J. Am. Chem. Soc.* **2013**, *135*, 10942 – 10945; b) J. K. Gao, J. W. Miao, P. Z. Li, W. Y. Teng, L. Yang, Y. L. Zhao, B. Liu, Q. C. Zhang, *Chem. Commun.* **2014**, *50*, 3786 – 3788; c) W. T. Xu, L. Ma, F. Ke, F. M. Peng, G. S. Xu, Y. H. Shen, J. F. Zhu, L. G. Qiu, Y. P. Yuan, *Dalton Trans.* **2014**, *43*, 3792 – 3798.
[13] K. T. Butler, C. H. Hendon, A. Walsh, *J. Am. Chem. Soc.* **2014**, *136*, 2703 – 2706.
[14] M. Grätzel, *Nature* **2001**, *414*, 338 – 344.
[15] a) Z. W. Zhu, F. Tao, F. Zheng, R. Chang, Y. M. Li, L. Heinke, Z. Liu, M. Salmeron, G. A. Somorjai, *Nano Lett.* **2012**, *12*, 1491 – 1497; b) E. A. Carbonio, M. J. Prieto, A. D. Siervo, R. Landers, *J. Phys. Chem. C* **2014**, *118*, 28679 – 28688; c) Z. J. Mei, Y. Li, M. H. Fan, L. Zhao, J. Zhao, *Chem. Eng. J.* **2015**, *259*, 293 – 302.
[16] Q. Li, B. D. Guo, J. G. Yu, J. R. Ran, B. H. Zhang, H. J. Yan, J. R. Gong, *J. Am. Chem. Soc.* **2011**, *133*, 10878 – 10884.
[17] T. J. Yu, Y. Zeng, J. P. Chen, Y. Y. Li, G. Q. Yang, Y. Li, *Angew. Chem. Int. Ed.* **2013**, *52*, 5631 – 5635; *Angew. Chem.* **2013**, *125*, 5741 – 5745.
[18] a) D. R. Sun, W. J. Liu, Y. H. Fu, Z. X. Fang, F. X. Sun, X. Z. Fu, Y. F. Zhang, Z. H. Li, *Chem. Eur. J.* **2014**, *20*, 4780 – 4788; b) Y. Kataoka, Y. Miyazaki, K. Sato, T. Saito, Y. Nakanishi, Y. Kiatagwa, T. Kawakami, M. Okumura, K. Yamaguchi, W. Mori, *Supramol. Chem.* **2011**, *23*, 287 – 296; c) C. Gomes Silva, I. Luz, F. X. Llabrés i Xamena, A. Corma, H. García, *Chem. Eur. J.* **2010**, *16*, 11133 – 11138; d) Y. Horiuchi, T. Toyao, M. Saito, K. Mochizuki, M. Iwata, H. Higashimura, M. Anpo, M. Matsuoka, *J. Phys. Chem. C* **2012**, *116*, 20848 – 20853; e) T. H. Zhou, Y. H. Du, A. Borgna, J. D. Hong, Y. B. Wang, J. Y. Han, W. Zhang, R. Xu, *Energy Environ. Sci.* **2013**, *6*, 3229 – 3234.
[19] M. Dai, X. R. Su, X. Wang, B. Wu, Z. G. Ren, X. Zhou, J. P. Lang, *Cryst. Growth Des.* **2014**, *14*, 240 – 248.

Received: September 9, 2015
Published online: January 6, 2016

